

Dr. Seg: Revisiting GRPO Training for Visual Large Language Models through Perception-Oriented Design

Haoxiang Sun¹ Tao Wang^{1†} Chenwei Tang¹ Li Yuan² Jiancheng Lv¹

¹College of Computer Science, Sichuan University

²School of Electronic and Computer Engineering, Peking University

haoxiang0311@gmail.com, twangnh@gmail.com

Abstract

Following the success of Group Relative Policy Optimization (GRPO) in foundation LLMs, an increasing number of works have sought to adapt GRPO to Visual Large Language Models (VLLMs) for visual perception tasks (e.g., detection and segmentation). However, much of this line of research rests on a long-standing yet unexamined assumption: training paradigms developed for language reasoning can be transferred seamlessly to visual perception. Our experiments show that this assumption is not valid, revealing intrinsic differences between reasoning-oriented and perception-oriented settings. Using reasoning segmentation as a representative case, we surface two overlooked factors: (i) the need for a broader output space, and (ii) the importance of fine-grained, stable rewards. Building on these observations, we propose Dr. Seg, a simple, plug-and-play GRPO-based framework consisting of a Look-to-Confirm mechanism and a Distribution-Ranked Reward module, requiring no architectural modifications and integrating seamlessly with existing GRPO-based VLLMs. Extensive experiments demonstrate that Dr. Seg improves performance in complex visual scenarios while maintaining strong generalization. Code, models, and datasets are available at <https://github.com/eVI-group-SCU/Dr-Seg>.

1. Introduction

Visual segmentation is a fundamental task in computer vision and has traditionally been dominated by specialist models [11, 19, 43]. In recent years, Visual Large Language Models (VLLMs) have demonstrated strong visual understanding capabilities through large-scale vision-language pretraining [1, 5, 14, 20]. By further applying instruction tuning on specially curated datasets, VLLMs have extended their capabilities to more complex and fine-grained perception tasks [17, 27, 47].

[†]Corresponding author.

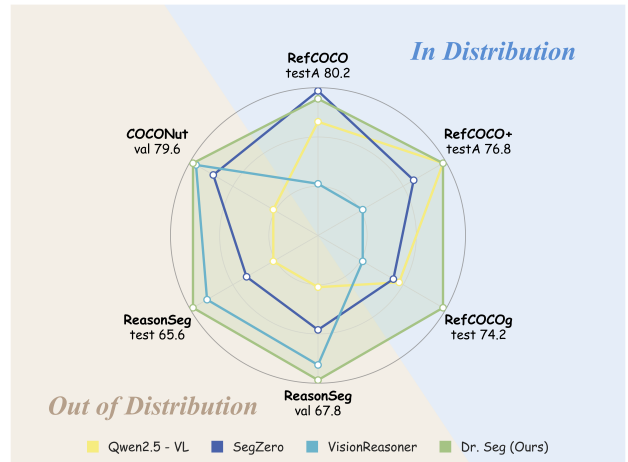


Figure 1. Dr. Seg achieves new state-of-the-art results on 5 out of 6 benchmarks under both in-distribution (ID) and out-of-distribution (OOD) conditions, demonstrating strong generalization ability.

Early attempts have further extended the capabilities of VLLMs towards reasoning-oriented segmentation, enhancing their flexibility and practical applicability [16, 48, 49]. Despite these advances, models that rely solely on instruction tuning exhibit limited generalization and are prone to catastrophic forgetting of general capabilities [24]. Recent studies, inspired by DeepSeek’s Group Relative Policy Optimization (GRPO) [32] method, have begun to adapt Reinforcement Learning with Verifiable Rewards (RLVR) to VLLMs in the post-training stage for a variety of vision tasks [24, 25, 33]. Despite differences in motivation and application domains, these methods generally follow a common pattern: they conduct post-training on VLLMs, curate task-specific datasets, and design reward functions to achieve performance improvements on targeted tasks. These efforts have led to substantial gains in the generalization of vision tasks, opening up new directions.

However, we find that directly transferring training strategies from reasoning-oriented tasks to perception-oriented tasks is not optimal. The suboptimality is rooted in

fundamental differences in learning dynamics and reward design: (i) perception-oriented tasks inherently require a broader output space to accommodate more diverse visual information, whereas reasoning-oriented tasks are driven by causal chains that naturally induce depth-oriented exploration within a narrower output space; and (ii) perception-oriented tasks demand fairer, better-calibrated rewards to reduce interference and noise among multiple optimization objectives. We thus aim to develop more effective learning methods that encourage broader output space exploration and provide finer reward feedback.

To this end, we introduce Dr. Seg, a simple yet effective GRPO-based framework for VLLMs, specifically tailored for visual perception tasks. Dr. Seg is built upon two key components. First, it integrates a Look-to-Confirm strategy that explicitly broadens the output search space: the model is encouraged to show its focus on certain visual information during reasoning, thus it is forced to look for plausible visual cues before confirming its final decision. This design promotes breadth-oriented exploration by enabling the model to derive reasoning paths from diverse dimensions (e.g., shape, material, relations) within its pre-trained visual knowledge, and in turn yields stronger generalization. Second, it incorporates a Distribution-Ranked Reward mechanism that provides fine-grained and adaptive feedback by tracking performance variations across training steps, while being robust to heterogeneity in metric scales, thus guiding the model toward more precise and stable improvements. *Together, these two components reinforce each other, with finer-grained reward to learn more accurate prediction under the wider output exploration space, yielding gains that go beyond the sum of their individual contributions.* Notably, Dr. Seg requires no modifications to the underlying model architecture, making it both lightweight and broadly applicable. It outperforms prior work on core vision tasks including referring expression comprehension and segmentation, object detection, reasoning segmentation and counting, e.g., compared to the baseline method, Dr. Seg achieves improvements of 2.0 absolute gIoU for ReasonSeg-test segmentation benchmark, 2.4 absolute AP for COCO detection benchmark and 4.5 for Pixmo-val counting benchmark.

In summary, our contributions are as follows:

- We identify key differences in GRPO training for visual perception tasks and reasoning tasks, i.e., output space and reward designs, and present a detailed analysis.
- We design a Look-to-Confirm strategy and Distribution-Ranked Reward mechanism, which are integrated to form a plug-and-play Dr. Seg method and collaboratively enhance the learning of visual perception in VLLMs.
- We present a challenging COCONut dataset to evaluate multi-object perception. Extensive experiments show that Dr. Seg achieves superior performance on multiple perception tasks while preserving robust generalization.

2. Related Work

Reasoning Segmentation with VLLMs. The emergence of Visual Large Language Models has significantly advanced visual understanding by combining perception with their inherent reasoning capabilities [1, 5, 14]. Many existing works leverage the next-token prediction paradigm by generating special tokens to guide a mask decoder for segmentation, inevitably requiring supervised fine-tuning (SFT) [16, 28, 30, 40, 48]. Another line of research generates prompts (e.g., boxes or points) to guide SAM [15], thereby offering greater flexibility [24, 25, 36]. Our work builds upon the latter approach, aiming to preserve both simplicity and flexibility.

Reinforcement Learning in VLLMs. Following the success of DeepSeek-R1 [12], a series of works have explored reinforcement learning methods in multimodal domains. Perception-R1 [44] and VisionReasoner [25] address multiple perception-oriented tasks and apply GRPO during post-training. In parallel, Seg-Zero [24], VLM-R1 [33], VersaVid-R1 [3], and CrowdVLM-R1 [38] focus on their respective domains. In this work, we focus on the task of Reasoning Segmentation, which serves as a representative setting that simultaneously requires reasoning ability to identify the correct target and perceptual precision to perform accurate segmentation.

Entropy and Output Space Dynamics in RL. Recently, a line of studies has begun to investigate where the performance gains in RL truly originate. Chu et al. [6] argue that SFT primarily enables memorization, while RL serves to generalize this ability. Liu et al. [21] and Wu et al. [39] both investigate the capability boundaries of RL, yet arrive at divergent conclusions regarding whether RL can transcend the capability space established during pre-training. Another line of work has explored the entropy perspective. Cui et al. [7] analyze entropy dynamics during training and propose an empirical law, while Wang et al. [37] reveal that high-entropy tokens play a significant role in the learning process. However, these studies are limited to reasoning-oriented scenarios, whereas our work is, to the best of our knowledge, the first to examine entropy dynamics from the perspective of perception-oriented tasks.

3. Revisiting GRPO for Visual Perception

In this section, we present our findings on the GRPO training process of visual large language models, identifying the differences and challenges w.r.t. reasoning-oriented tasks.

3.1. Preliminaries

Group Relative Policy Optimization. Given a query q , the policy model $\pi_{\theta_{\text{old}}}$ samples a group of candidate outputs o_1, o_2, \dots, o_G for each input. The policy is then optimized

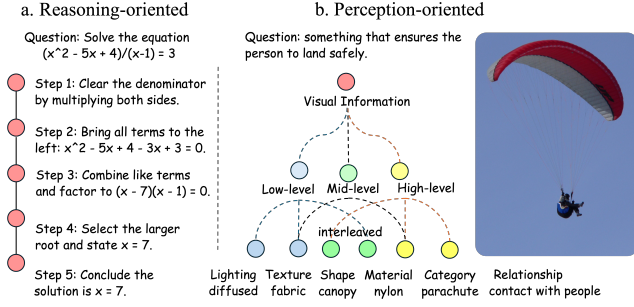


Figure 2. Illustration of breadth-oriented exploration in perception-oriented tasks. Multiple level visual attributes can support different reasoning trajectories.

by maximizing the following objective:

$$J_{\text{GRPO}}(\theta) = \mathbb{E}_{q \sim P(Q), \{o_i\}_{i=1}^G \sim \pi_{\theta_{\text{old}}}(O|q)} \left[\frac{1}{G} \sum_{i=1}^G \min(s_1 A_i, s_2 A_i) - \beta D_{\text{KL}}(\pi_{\theta} \parallel \pi_{\text{ref}}) \right],$$

$$s_1 = \frac{\pi_{\theta}(o_i|q)}{\pi_{\theta_{\text{old}}}(o_i|q)}, \quad s_2 = \text{clip}(s_1, 1 - \epsilon, 1 + \epsilon).$$

where ϵ and β are the PPO clipping hyper-parameter and the coefficient controlling the KL penalty [31]. A_i is the computed advantage using the group rewards $\{r_1, r_2, \dots, r_G\}$, normalized within each group.

$$A_i = \frac{r_i - \text{mean}(\{r_1, r_2, \dots, r_G\})}{\text{std}(\{r_1, r_2, \dots, r_G\})}$$

Reward Composition. In our settings, for each candidate output o_i , the total reward is composed of two parts: a format reward $r_{\text{fmt}}(o_i)$, which evaluates whether the output conforms to the required structure, and an accuracy reward $r_{\text{acc}}(o_i)$, which measures the alignment between the predicted boxes/points and the ground-truth. The final reward is defined as the sum of the two:

$$r_i = r_{\text{fmt}}(o_i) + r_{\text{acc}}(o_i),$$

3.2. Exploration Path and Entropy Fluctuations

Unlike reasoning-oriented tasks [7, 37], we assume that visual perception tasks naturally favor breadth-first exploration. Specifically, in reasoning-oriented settings such as mathematics and other scientific domains, the conclusions are tightly constrained by the preceding premises. Such a structure naturally favors depth-oriented exploration and tends to narrow the output search space. By contrast, perception-oriented tasks do not fundamentally rely on such rigid ordering and are inherently characterized by a much more diverse information landscape. For a given answer, the model can follow many different reasoning trajectories:

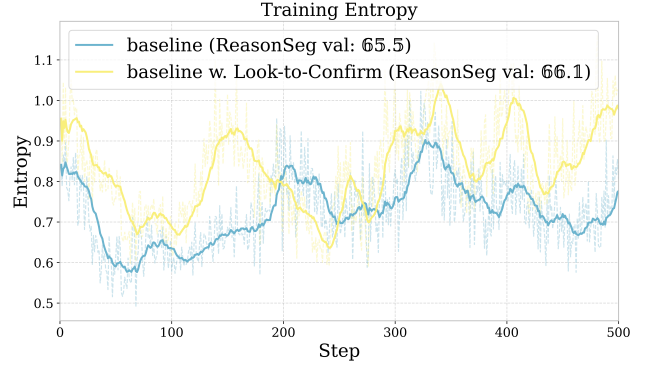


Figure 3. Comparison of token-level entropy during training between baseline VisionReasoner[25] model and baseline with a Look-to-Confirm strategy introduced in the next section. The numbers in parentheses are the performance on ReasonSeg dataset.

it may ground its decision in low-level cues such as lighting and texture, in mid-level visual attributes such as shape, color, and material, or in higher-level semantic information such as object categories and their spatial relations. And there could be combinations between different levels of information. Many of these diverse reasoning paths can ultimately lead to the correct answer. We provide an example in Fig. 2.

We further examine the model’s entropy to corroborate this hypothesis. Following prior work [7, 37], we plot the training-time token-level average entropy and find that it remains highly unstable, which indicates the model is uncertain for its token outputs during the training, resulting in broader exploration paths. This is in sharp contrast to recent RLVR reports on reasoning-oriented settings that document a smooth, monotonic descent [7, 37], as shown in Fig. 3. We find that encouraging such breadth exploration in the reasoning process can improve performance (66.1 vs. 65.5 in ReasonSeg task), with the entropy fluctuating even more substantially, i.e., the yellow curve in Fig. 3. Furthermore, the embeddings are markedly more dispersed with such encouragement, as shown in Fig. 4. The detailed breadth-encouraging strategy named Look-to-Confirm is presented in the next section. This behavior indicates that, as training progresses, the policy does not collapse into a narrow region of the output space during its exploration.

3.3. The Pitfall in Reward Design

In addition to the above analysis of the exploration path, the reward design also requires detailed inspection. Most prior work on VLLM-based perception adopts the binary rewards popular in reasoning tasks [24, 25, 36]. This is counterintuitive for vision, where metrics such as IoU are inherently continuous and thus enable finer reward feedback; collapsing them to binary signals appears unnecessarily lossy. A

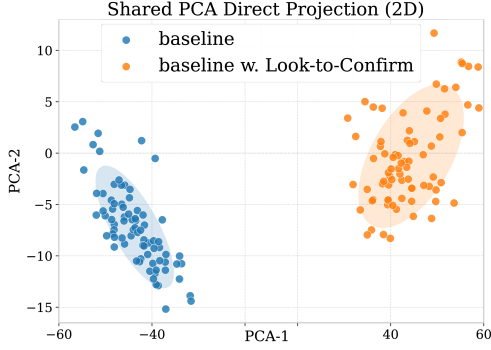


Figure 4. PCA visualization of last-token embeddings for baseline VisionReasoner[25] model vs. baseline with Look-to-Confirm. Points are 2D projections; shaded ellipses denote 2σ covariance contours around each group mean.

Table 1. Evaluation metrics of the baseline and the raw reward setting. Although the model achieves improved performance on the simpler RefCOCO, RefCOCO+, and RefCOCog benchmarks, its performance degrades on the more challenging ReasonSeg benchmark, which features a mixture of single- and multi-object cases.

Method	RCO	RCO+	RCOg	ReasonSeg
Baseline	79.0	75.3	72.5	65.5
Raw reward	80.0	76.3	74.0	64.7

natural next step is to apply raw, unnormalized continuous rewards¹. However, as shown in Fig. 1, we find that when multiple optimization targets are involved simultaneously, simply using the final reward as the sum of N different accuracy rewards introduces bias, which in turn causes policy optimization to suffer from suboptimality.

We provide a mathematical explanation showing that the gradient is sensitive to the intrinsic scales of individual reward components $r^{(j)}$; high-variance components dominate the update while low-variance components are suppressed. We assume component-wise finite second moments for the reward vector. For a given query q and output o , let the N -dimensional reward vector be $\mathbf{r} := (r^{(1)}, \dots, r^{(N)})^\top$ with mean vector $\boldsymbol{\mu} = (\mu^{(1)}, \dots, \mu^{(N)})^\top$ and covariance matrix $\Sigma = [\sigma^{(jk)}]_{j,k=1}^N$, where $\sigma^{(jk)} = \text{Cov}(r^{(j)}, r^{(k)})$. The total scalar reward is

$$r = \sum_{j=1}^N r^{(j)} \quad (4)$$

Let $\mu_r := \mathbb{E}[r]$ and $\sigma_{\text{mix}}^2 := \text{Var}(r) = \mathbf{1}^\top \Sigma \mathbf{1}$ denote the mixed mean and variance of all N reward components into a single scale. Under the standard GRPO normalization $A = (r - \mu_r) / \sigma_{\text{mix}}$, omitting clipping, KL penalties, and importance ratio terms in a simplified form, the surrogate

¹More experiment details in supplementary materials.

policy gradient can be derived from Eq. 1, written as:

$$g(\theta; q) = \frac{1}{\sigma_{\text{mix}}} \mathbb{E}[(r - \mu_r) S] = \frac{1}{\sigma_{\text{mix}}} \text{Cov}(r, S), \quad (5)$$

where $S = \nabla_{\theta} \log \pi_{\theta}(o | q)$ is the score function of the policy. Expanding the reward into components and rewriting each covariance term via its correlation coefficient, the gradient can be rewritten as:

$$g(\theta; q) = \frac{1}{\sigma_{\text{mix}}} \sum_{j=1}^N \text{Cov}(r^{(j)}, S) = \frac{\sigma_S}{\sigma_{\text{mix}}} \sum_{j=1}^N \rho^{(j)} \sigma^{(j)} \quad (6)$$

where

$$\text{Cov}(r^{(j)}, S) = \rho^{(j)} \sigma^{(j)} \sigma_S \quad (7)$$

σ_S and $\sigma^{(j)}$ are the standard deviations of S and $r^{(j)}$; $\rho^{(j)}$ denotes the Pearson correlation coefficient between $r^{(j)}$ and S . Since σ_S and σ_{mix} are common to all dimensions and simply rescale the gradient, we focus on $\rho^{(j)} \sigma^{(j)}$ —and, for components with comparable $\rho^{(j)}$, the variance term $\sigma^{(j)}$ alone determines their relative weight. Thus $\sigma^{(j)}$ biases the effective weighting of each reward dimension. *In particular, high-variance components $\sigma^{(j)}$ induce larger covariance with S and therefore dominate the mixed gradient, while low-variance components are relatively suppressed.*

4. Method

To overcome the above limitations, we propose Dr. Seg, a GRPO-based method to enhance VLLMs for visual perception tasks. It comprises two key components: a Look-to-Confirm strategy to enlarge the output space and a Distribution-Ranked Reward mechanism for fine-grained, stable rewards. The integration of the two components enables mutual enhancement of richer exploration path and stabler reward feedback, leading to much higher performance.

4.1. Architecture

Following VisionReasoner [25], Dr. Seg decouples the reasoning process from the segmentation process. We only train the VLLM, which is prompted to generate a set of boxes and points for each target object. These predicted boxes and points are then used to compute rewards and provide feedback during training under the GRPO [32] framework. At evaluation time, the boxes and points produced by the VLLM are used as prompts to drive SAM2 [29] for segmentation.

4.2. Look-to-Confirm Visual Exploration

To encourage breadth exploration, we incorporate a visual exploration process into the reasoning path. Concretely, we

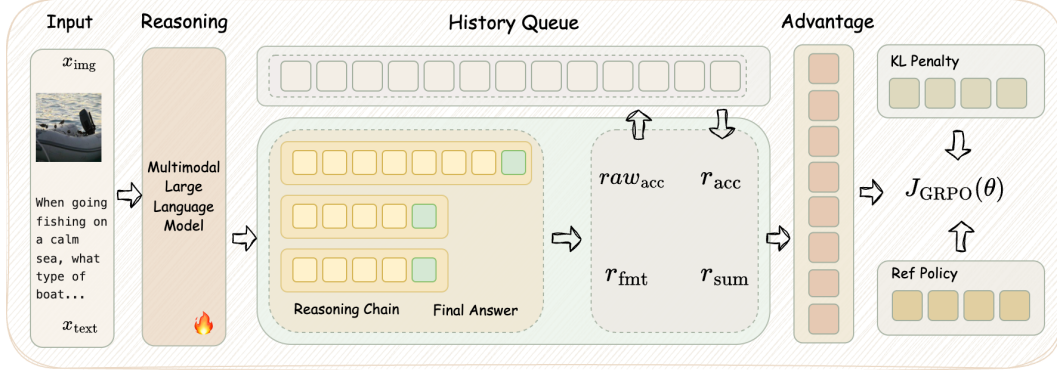


Figure 5. Overall training pipeline of Dr. Seg.

User Prompt for Dr. Seg

"Please find "**{Question}**" with bboxes and points."
 "Compare the difference between object(s) and find the most closely matched object(s)."
 "Output the thinking process inside `<think>...</think>`."
 "Inside this reasoning, you must include one or more `<look>...</look>` blocks, enclosing the parts of the reasoning where you pay special attention to certain visual information."
 "Then, output the final answer inside `<answer>...</answer>`."
 "Output the bbox(es) and point(s) inside the interested object(s) in JSON format."
 "i.e., `<think>` [your reasoning text]
`<look>` [your visual focus] `</look>` [more reasoning text] `</think>`"
`<answer>` { [{"bbox_2d": [10,100,200,210], "point_2d": [30,110]}, {"bbox_2d": [225,296,706,786], "point_2d": [302,410]}] `</answer>`"

Figure 6. User prompt for Dr. Seg.

prompt the model to explicitly mark salient visual evidence with a `<look>` tag. As presented in Fig. 6, the model is prompted to use `<look>` tags to explicitly enclose the parts of the reasoning that require special attention to visual information, and we assign a corresponding format reward to encourage adherence to this structure. This way, the model is forced to show its focus on certain visual information during reasoning, thus it looks for plausible visual cues from diverse perspectives with its pre-trained visual knowledge, e.g., looking at evidence such as shape specifics, material, spatial relations, thereby obtaining stronger generalization. This is inspired by Yang et al. [42], who study the effect of explicitly injecting a reflection and verification process into model reasoning by inserting a `<back>` phase. Unlike their approach, we take the perspective of expanding the output search space, only asking the model to look over the image space, without performing any additional verification of its answers.

In addition, we follow prior work [24, 25] and incorporate three additional format-related rewards and obtain the total format reward:

$$r_{\text{fmt}}(o_i) = r_{\text{look}}(o_i) + r_{\text{think}}(o_i) + r_{\text{ans}}(o_i) + r_{\text{nr}}(o_i) \quad (8)$$

Specifically, r_{look} is 1.0 if the reasoning trace includes `<look>...</look>`. r_{think} is 1.0 if the model outputs a thinking trace enclosed by `<think> ...</think>` and places the final answer within `<answer> ...</answer>`. r_{ans} is 1.0 if the final answer conforms to the restricted JSON format with correct key-value pairs. r_{nr} is 1.0 if the thinking trace is unique and non-repetitive.

4.3. Distribution-Ranked Accuracy Reward

Overview and Quantile Mapping. To address the high-variance dominance problem, we develop a quantile mapping strategy. We maintain a fixed-length FIFO queue that stores recent accuracy vectors to approximate the empirical distribution of each metric. When computing the reward for a new output, each raw metric value is mapped to its empirical quantile (rank) within the queue, yielding a scale-invariant score. Specifically, given a candidate output o_i , we first define an N -dimensional raw accuracy vector, where each dimension corresponds to a perception-oriented evaluation metric:

$$\mathbf{x}(o_i) = (x_1, x_2, \dots, x_N) \in [0, 1]^N \quad (9)$$

To obtain a scale-invariant and rank-based score comparable across batches, each component x_j is mapped to its empirical quantile q_j with respect to a FIFO rolling history queue $\mathcal{S}_t^{(j)} = (s_1^{(j)}, \dots, s_M^{(j)})$ maintained at training step t :

$$q_j = \frac{1}{M} \sum_{m=1}^M \mathbf{1}(s_m^{(j)} \leq x_j), \quad (10)$$

$$\mathbf{q}(o_i) = (q_1, \dots, q_N) \in [0, 1]^N, \quad (11)$$

where $\mathbf{1}(\cdot)$ is the indicator function. By constructing this per-dimension Empirical Cumulative Distribution Function (ECDF) [9], the mapping $T : \mathbf{x} \mapsto \mathbf{q}$ is coordinatewise monotone, bounded, and time-varying.

Final Reward Aggregation. The final distribution-ranked accuracy reward r_{acc} is aggregated across the N quantile scores:

$$r_{\text{acc}}(o_i) = \frac{1}{N} \sum_{j=1}^N q_j, \quad (12)$$

yielding a robust, time-adaptive scalar reward that reflects the relative standing of o_i under the evolving performance distribution. Importantly, our FIFO-queue-based normalization maps each raw accuracy component x_j to an empirical quantile $q_j \in [0, 1]$, i.e., to its rank within the recent history of that metric. This rank-based, history-relative scale decouples each component’s effective gradient scale from its raw numerical magnitude: the difficulty of a sample is determined by its position in the evolving performance distribution rather than by the absolute value, as validated by our experiments.

Specialization ($N = 3$). To obtain fine-grained reward, in our VLLM setting, the raw accuracy vector \mathbf{x} comprises three essential perception metrics: x_1 measures the alignment between the predicted bounding boxes b_{pred} and ground-truth bounding boxes b_{gt} (IoU).

$$x_1 = \text{IoU}(b_{\text{pred}}, b_{\text{gt}}) \quad (13)$$

x_2 evaluates the prediction coverage consistency based on the counts of predicted N_{pre} and ground-truth objects N_{gt} .

$$x_2 = \frac{\min(N_{\text{pre}}, N_{\text{gt}})}{\max(N_{\text{pre}}, N_{\text{gt}})}, \quad (14)$$

x_3 quantifies the similarity between the predicted points p_{pred} and ground-truth points p_{gt} . Let $d_{\text{pt}} = \|p_{\text{pred}} - p_{\text{gt}}\|_2$ denote their Euclidean distance; we then define

$$x_3 = g(d_{\text{pt}}), \quad (15)$$

$$g(d_{\text{pt}}) = \begin{cases} 1, & d_{\text{pt}} \leq \tau_{\min}, \\ \frac{\tau_{\max} - d_{\text{pt}}}{\tau_{\max} - \tau_{\min}}, & \tau_{\min} < d_{\text{pt}} < \tau_{\max}, \\ 0, & d_{\text{pt}} \geq \tau_{\max}. \end{cases} \quad (16)$$

τ_{\min} and τ_{\max} define the bounds of the soft penalty region for the point guidance signal.

5. Experiments

5.1. Experiment Setup

Datasets and Evaluation Benchmarks. Following [25], we adopt the same datasets and preparation strategy. The training dataset *VisionReasoner_multi_object_7k_840* is constructed from four sources: LVIS [13], RefCOCOg [45], gRefCOCO [19], and LISA++ [41], resulting in approximately 7,000 training samples in total; refer to supplementary materials for more details. For evaluation, we follow prior work [24, 25, 36] and report gIoU, defined as the mean IoU across all segmentation masks. We adopt

the same data splits as [24, 25, 36] across RefCOCO, RefCOCO+, RefCOCOg, and ReasonSeg, totaling approximately 10,000 samples for a fair comparison. The first three datasets serve as in-distribution benchmarks for referring expression segmentation, whereas ReasonSeg serves as the out-of-distribution benchmark for reasoning segmentation.

We additionally construct an evaluation setting to further assess multi-object segmentation. Specifically, we sample 665 images from the COCONut panoptic segmentation dataset [10], selecting scenes that require segmenting multiple objects simultaneously. The resulting split contains an average of 5.14 target object instances per image and spans 68 categories, all within the original COCO taxonomy. Further details of the construction protocol are provided in the supplementary material.

Running Quantile Estimator. For the distribution-ranked accuracy reward, we employ a quantile service that maintains a fixed-length FIFO queue of size 2,048, corresponding to the historical accuracy records from the past 16 training steps. We initialize the queue with a full step of zeros before inserting actual records. In practice, at each rollout, raw accuracy vectors from candidate outputs are first pushed into a temporary buffer, which is then flushed into the global queue at the end of each training step.

Implementation Details. We train Dr. Seg under the VERL [34] framework, employing Qwen2.5-VL-7B [1] and SAM2-Large [29] as the reasoning and segmentation models, respectively. Dr. Seg is initialized with settings similar to VisionReasoner [25]. We use a batch size of 16 and a learning rate of 1×10^{-6} . All training is conducted on 4 NVIDIA H800 GPUs for around 500 steps. For the distance-based reward mapping function $g(\cdot)$, we set the lower threshold to 30 and the upper threshold to 200.

5.2. Main Results

We evaluate Dr. Seg against state-of-the-art VLLMs, including LISA [16], GLaMM [28], PixelLM [30], GSVA [40], OMG-LLaVa [48], Seg-Zero [24], VisionReasoner [25], Pixel-Think [36], Qwen2-VL [35], Qwen2.5-VL [1]. We also compare task-specific models, including LAVT [43] and ReLA [19]. For models that do not report gIoU, we use their cIoU reported in [25] as an alternative.

As shown in Tab. 2, Dr. Seg consistently achieves state-of-the-art performance across 5/6 benchmarks, outperforming other models in its class. Notably, while prior studies [24, 25] often attained state-of-the-art performance in either in-distribution or out-of-distribution environments alone, our model achieves new state-of-the-art results in both simultaneously. We attribute this superior performance to the task-specific design tailored for perception-oriented settings, where our two proposed improvements work synergistically. Refer to the supplementary material for qualitative results.

Table 2. Performance on in-distribution (ID) and out-of-distribution (OOD) benchmarks. † indicates that the code was not open-sourced as of the submission deadline. *denotes results obtained from our independent experiments under the same experimental conditions. RCO, RCO+, and RCOg refer to RefCOCO, RefCOCO+, and RefCOCOg, respectively. - denotes not available.

Method	In Distribution				Out of Distribution				Total
	RCO	RCO+	RCOg	ID avg	ReasonSeg	COCONut	OOD avg	avg	
	<i>testA</i>	<i>testA</i>	<i>test</i>		<i>val</i>	<i>test</i>			<i>val</i>
Task-specific Models									
LAVT [43]	75.8	68.4	62.1	68.8	-	-	-	-	
ReLA [19]	76.5	71.0	66.5	71.3	22.4	21.3	-	-	
Base 7B Models									
Qwen2-VL [35]	68.7	65.7	63.5	66.0	44.5	38.7	9.8*	31.0	46.9
Qwen2.5-VL [1]	79.9	76.8	72.8	76.5	56.9	52.1	31.8*	45.5	61.7
SFT-based 7B VLLMs									
LISA [16]	76.5	67.4	68.5	70.8	44.4	36.8	-	-	-
GLaMM [28]	58.1	47.1	55.6	53.6	-	-	-	-	-
PixelLM [30]	76.5	71.7	70.5	72.9	-	-	-	-	-
GSVA [40]	78.9	69.6	73.3	73.9	-	-	-	-	-
OMG-LLaVa [48]	79.8	73.0	71.9	74.9	-	-	-	-	-
RL-based 7B VLLMs									
Seg-Zero [24]	80.3	76.2	72.6	76.4	62.6	57.5	69.3*	63.1	69.8
Pixel-Think† [36]	79.3	74.8	73.9	76.0	63.8	60.2	-	-	-
VisionReasoner [25]	78.9	74.9	71.3	75.0	66.3	63.6	78.1*	69.3	72.2
VisionReasoner*	79.0*	75.3*	72.5*	75.6	65.5*	61.5*	78.1*	68.4	72.0
Dr. Seg (Ours)	80.2	76.8	74.2	77.1	67.8	65.6	79.6	71.0	74.0

5.3. Additional Task Results

To further assess the effectiveness and generality of our approach, we additionally evaluate Dr. Seg on object detection and counting under the same experimental settings as VisionReasoner [25]. For detection, we use COCO [18]. For counting, we use PixMoCount [8] and CountBench [26]. As shown in Tab. 3, our method also achieves state-of-the-art.

Table 3. Performance on Detection and Counting tasks. We approximate COCO AP using the ratio of the bounding box area to the total image area to enable compatibility with COCOAPI.

Method	Detection	Counting		
	COCO	Pixmo	Count	
	<i>val</i>	<i>val</i>	<i>test</i>	<i>test</i>
Qwen2-VL [35]	28.3	29.9	48.0	76.5
Qwen2.5-VL [1]	29.2	63.3	67.9	76.0
VisionReasoner [25]	37.7	70.1	69.5	87.6
Dr. Seg (Ours)	40.1	74.6	72.4	91.5

5.4. Ablation Study

We conduct ablation experiments to disentangle the contributions of different components in Dr. Seg.

Effect of Look-to-Confirm and Distribution-Ranked Reward. We conduct an ablation study to disentangle the contributions of our two proposed components: (i) enforcing the <look> format and (ii) adopting the distribution-ranked accuracy reward. Tab. 4 reports results under four settings.

Table 4. Ablation study on Look-to-Confirm and Distribution-Ranked Reward. LC and DR refer to Look-to-Confirm and Distribution-Ranked Reward, respectively.

LC	DR	RCO	RCO+	RCOg	ReasonSeg
		79.0	75.3	72.5	65.5
✓		79.0	75.1	72.1	66.1
	✓	80.1	76.6	73.9	65.5
✓	✓	80.2	76.8	74.2	67.8

The ablation results reveal the difference between the two modules. Look-to-Confirm encourages a broader output space during training, enhancing the model’s ability to generalize better on the out-of-distribution reasoning segmentation task, which requires more complex visual reasoning than training data, i.e., a 0.6 point improvement on ReasonSeg task. Yet due to the coarse binary reward, the learning of continuous predictions such as bounding boxes is affected, resulting in slightly reduced performance

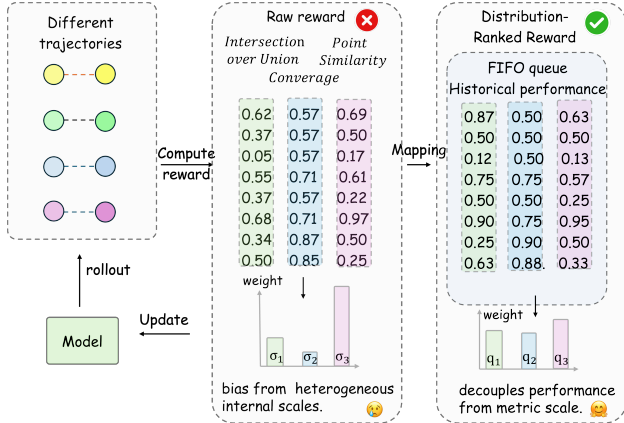


Figure 7. A snapshot of sample training rewards. Our Distribution-Ranked Reward maps each reward component to an empirical quantile $\mathbf{q} = [q_1, q_2, q_3] \in [0, 1]^3$ using a FIFO history queue, obtaining rank-based score that is scale-invariant and overcoming high-variance domination.

on the in-distribution accuracy. Distribution-Ranked Reward, on the other hand, improves in-distribution performance, i.e., 1.1, 1.5 and 1.8 absolute IoU gains on the RefCOCO, RefCOCO+, RefCOCog, respectively. This indicates that it provides stable, fine-grained signals that improve the model’s data fitting capability. However, since there is no regularization encouraging the output space exploration, the out-of-distribution ReasonSeg performance is not improved. Surprisingly, when the two mechanisms are combined, they work synergistically together, unlocking marked enhancement on both in-distribution and out-of-distribution tasks, demonstrating both the effectiveness of our design and the synergy between the two components. **Effect of Normalization.** To isolate the contribution of our distribution-ranked normalization mechanism, we compare two settings under the same reward formulation: (i) directly applying raw, unnormalized continuous rewards, and (ii) applying distribution-ranked normalization through the FIFO queue. As shown in Tab. 5, the raw reward setting leads to a substantial degradation, which is consistent with our previous observations. We also present a snapshot of training rewards with rank-based normalization in Fig. 7, showing its effectiveness.

Table 5. Ablation on normalization strategy.

Normalization	RCO	RCO+	RCOg	ReasonSeg
Raw Reward	78.7	75.0	71.5	64.4
Distribution-Ranked	80.2	76.8	74.2	67.8

Effect of Queue Size. We vary the FIFO queue size for Distribution-Ranked Reward normalization. As shown in Tab. 6, larger queues yield more stable and consistent gains

on ID benchmarks. However, when the queue becomes too long, OOD performance starts to degrade—resembling the behavior of the raw-reward setting. We speculate that an overly long history queue makes the baseline overly stable: exploring new breadth directions naturally induces short-term performance fluctuations over several neighboring steps, and this over-stabilized design instead suppresses such exploration.

Table 6. Ablation on queue size (numbers in parentheses indicate past steps).

Queue Size	RCO	RCO+	RCOg	ReasonSeg
128 (1)	80.1	76.0	73.6	63.3
512 (4)	80.0	76.3	73.6	66.3
2048 (16)	80.2	76.8	74.2	67.8
8192 (64)	80.4	77.3	74.3	65.2

6. Conclusion

In this work, we revisit VLLM training for perception-oriented vision tasks and identify two overlooked aspects of current research: the entropy instability inherent to visual exploration and inappropriate reward design. Based on our analysis, we propose Dr. Seg, a simple GRPO-based framework integrating a Look-to-Confirm mechanism and a Distribution-Ranked Reward module. Without any architectural modifications, Dr. Seg obtains state-of-the-art performance on a wide range of perception tasks such as referring segmentation and object detection. Meanwhile, it achieves strong generalization to out-of-distribution scenarios. Our work reveals the importance of perception-oriented design in both reasoning patterns and reliable rewards.

Limitations and Future Work. While effective, our study is limited to a subset of the broad vision tasks. Thus, how to transfer our method to other tasks (e.g., tracking, pose estimation, and video understanding) or non-visual modalities (e.g., point cloud) remains open. Additionally, the method only implicitly introduces the visual augmentation in the reasoning process of VLLM, which introduces no explicit feature enrichment from visual modality and may not be optimal for the dense object-level visual perception tasks. Recent research has shown that explicit pathways such as spatially adaptive visual tokenization can effectively inject visual details and improve these core vision tasks. Thus synergistically combining both implicit and explicit visual injection remains future work.

Acknowledgment

This work is supported by the National Science Foundation of China under Grant 62506249, the National Major Scientific Instruments and Equipments Development Project of National Natural Science Foundation of China under Grant

62427820, the Natural Science Foundation of Sichuan under grant 2024NSFSC1462, and the Fundamental Research Funds for the Central Universities under grant YJ202342.

References

- [1] Shuai Bai, Keqin Chen, Xuejing Liu, Jialin Wang, Wenbin Ge, Sibao Song, Kai Dang, Peng Wang, Shijie Wang, Jun Tang, et al. Qwen2. 5-vl technical report. *arXiv preprint arXiv:2502.13923*, 2025. 1, 2, 6, 7, 4
- [2] Keqin Chen, Zhao Zhang, Weili Zeng, Richong Zhang, Feng Zhu, and Rui Zhao. Shikra: Unleashing multimodal llm’s referential dialogue magic. *arXiv preprint arXiv:2306.15195*, 2023. 4
- [3] Xinlong Chen, Yuanxing Zhang, Yushuo Guan, Bohan Zeng, Yang Shi, Sihan Yang, Pengfei Wan, Qiang Liu, Liang Wang, and Tieniu Tan. Versavid-r1: A versatile video understanding and reasoning model from question answering to captioning tasks. *arXiv preprint arXiv:2506.09079*, 2025. 2
- [4] Zhe Chen, Weiyun Wang, Hao Tian, Shenglong Ye, Zhangwei Gao, Erfei Cui, Wenwen Tong, Kongzhi Hu, Jiapeng Luo, Zheng Ma, et al. How far are we to gpt-4v? closing the gap to commercial multimodal models with open-source suites. *Science China Information Sciences*, 67(12):220101, 2024. 4
- [5] Zhe Chen, Jiannan Wu, Wenhai Wang, Weijie Su, Guo Chen, Sen Xing, Muyan Zhong, Qinglong Zhang, Xizhou Zhu, Lewei Lu, et al. Internvl: Scaling up vision foundation models and aligning for generic visual-linguistic tasks. In *Proceedings of the IEEE/CVF conference on computer vision and pattern recognition*, pages 24185–24198, 2024. 1, 2
- [6] Tianzhe Chu, Yuexiang Zhai, Jihan Yang, Shengbang Tong, Saining Xie, Dale Schuurmans, Quoc V Le, Sergey Levine, and Yi Ma. Sft memorizes, rl generalizes: A comparative study of foundation model post-training. *arXiv preprint arXiv:2501.17161*, 2025. 2
- [7] Ganqu Cui, Yuchen Zhang, Jiacheng Chen, Lifan Yuan, Zhi Wang, Yuxin Zuo, Haozhan Li, Yuchen Fan, Huayu Chen, Weize Chen, et al. The entropy mechanism of reinforcement learning for reasoning language models. *arXiv preprint arXiv:2505.22617*, 2025. 2, 3
- [8] Matt Deitke, Christopher Clark, Sangho Lee, Rohun Tripathi, Yue Yang, Jae Sung Park, Mohammadreza Salehi, Niklas Muennighoff, Kyle Lo, Luca Soldaini, et al. Molmo and pixmo: Open weights and open data for state-of-the-art vision-language models. In *Proceedings of the Computer Vision and Pattern Recognition Conference*, pages 91–104, 2025. 7, 2
- [9] Frederik Michel Dekking. *A Modern Introduction to Probability and Statistics: Understanding why and how*. Springer Science & Business Media, 2005. 5
- [10] Xueqing Deng, Qihang Yu, Ali Athar, Chenglin Yang, Linjie Yang, Xiaojie Jin, Xiaohui Shen, and Liang-Chieh Chen. Coconut-pancap: Joint panoptic segmentation and grounded captions for fine-grained understanding and generation. *arXiv preprint arXiv:2502.02589*, 2025. 6, 3
- [11] Henghui Ding, Chang Liu, Suchen Wang, and Xudong Jiang. Vision-language transformer and query generation for referring segmentation. In *Proceedings of the IEEE/CVF international conference on computer vision*, pages 16321–16330, 2021. 1
- [12] Daya Guo, Dejian Yang, Haowei Zhang, Junxiao Song, Ruoyu Zhang, Runxin Xu, Qihao Zhu, Shirong Ma, Peiyi Wang, Xiao Bi, et al. Deepseek-r1: Incentivizing reasoning capability in llms via reinforcement learning. *arXiv preprint arXiv:2501.12948*, 2025. 2
- [13] Agrim Gupta, Piotr Dollar, and Ross Girshick. Lvis: A dataset for large vocabulary instance segmentation. In *Proceedings of the IEEE/CVF conference on computer vision and pattern recognition*, pages 5356–5364, 2019. 6, 2
- [14] Aaron Hurst, Adam Lerer, Adam P Goucher, Adam Perelman, Aditya Ramesh, Aidan Clark, AJ Ostrow, Akila Welihinda, Alan Hayes, Alec Radford, et al. Gpt-4o system card. *arXiv preprint arXiv:2410.21276*, 2024. 1, 2
- [15] Alexander Kirillov, Eric Mintun, Nikhila Ravi, Hanzi Mao, Chloe Rolland, Laura Gustafson, Tete Xiao, Spencer Whitehead, Alexander C Berg, Wan-Yen Lo, et al. Segment anything. In *Proceedings of the IEEE/CVF international conference on computer vision*, pages 4015–4026, 2023. 2, 1
- [16] Xin Lai, Zhuotao Tian, Yukang Chen, Yanwei Li, Yuhui Yuan, Shu Liu, and Jiaya Jia. Lisa: Reasoning segmentation via large language model. In *Proceedings of the IEEE/CVF Conference on Computer Vision and Pattern Recognition*, pages 9579–9589, 2024. 1, 2, 6, 7
- [17] Zhaowei Li, Qi Xu, Dong Zhang, Hang Song, Yiqing Cai, Qi Qi, Ran Zhou, Junting Pan, Zefeng Li, Van Tu Vu, et al. Groundinggpt: Language enhanced multi-modal grounding model. *arXiv preprint arXiv:2401.06071*, 2024. 1
- [18] Tsung-Yi Lin, Michael Maire, Serge Belongie, James Hays, Pietro Perona, Deva Ramanan, Piotr Dollár, and C Lawrence Zitnick. Microsoft coco: Common objects in context. In *European conference on computer vision*, pages 740–755. Springer, 2014. 7, 2
- [19] Chang Liu, Henghui Ding, and Xudong Jiang. Gres: Generalized referring expression segmentation. In *Proceedings of the IEEE/CVF conference on computer vision and pattern recognition*, pages 23592–23601, 2023. 1, 6, 7, 2
- [20] Haotian Liu, Chunyuan Li, Qingyang Wu, and Yong Jae Lee. Visual instruction tuning. *Advances in neural information processing systems*, 36:34892–34916, 2023. 1
- [21] Mingjie Liu, Shizhe Diao, Ximing Lu, Jian Hu, Xin Dong, Yejin Choi, Jan Kautz, and Yi Dong. Prorl: Prolonged reinforcement learning expands reasoning boundaries in large language models. *arXiv preprint arXiv:2505.24864*, 2025. 2
- [22] Shilong Liu, Shijia Huang, Feng Li, Hao Zhang, Yaoyuan Liang, Hang Su, Jun Zhu, and Lei Zhang. Dq-detr: Dual query detection transformer for phrase extraction and grounding. In *Proceedings of the AAAI Conference on Artificial Intelligence*, pages 1728–1736, 2023. 4
- [23] Shilong Liu, Zhaoyang Zeng, Tianhe Ren, Feng Li, Hao Zhang, Jie Yang, Qing Jiang, Chunyuan Li, Jianwei Yang, Hang Su, et al. Grounding dino: Marrying dino with grounded pre-training for open-set object detection. In *European conference on computer vision*, pages 38–55. Springer, 2024. 4

- [24] Yuqi Liu, Bohao Peng, Zhisheng Zhong, Zihao Yue, Fanbin Lu, Bei Yu, and Jiaya Jia. Seg-zero: Reasoning-chain guided segmentation via cognitive reinforcement. *arXiv preprint arXiv:2503.06520*, 2025. 1, 2, 3, 5, 6, 7
- [25] Yuqi Liu, Tianyuan Qu, Zhisheng Zhong, Bohao Peng, Shu Liu, Bei Yu, and Jiaya Jia. Visionreasoner: Unified visual perception and reasoning via reinforcement learning. *arXiv preprint arXiv:2505.12081*, 2025. 1, 2, 3, 4, 5, 6, 7
- [26] Roni Paiss, Ariel Ephrat, Omer Tov, Shiran Zada, Inbar Mosseri, Michal Irani, and Tali Dekel. Teaching clip to count to ten. In *Proceedings of the IEEE/CVF International Conference on Computer Vision*, pages 3170–3180, 2023. 7, 2
- [27] Kanchana Ranasinghe, Satya Narayan Shukla, Omid Pour-saeed, Michael S Ryoo, and Tsung-Yu Lin. Learning to localize objects improves spatial reasoning in visual-llms. In *Proceedings of the IEEE/CVF Conference on Computer Vision and Pattern Recognition*, pages 12977–12987, 2024. 1
- [28] Hanoona Rasheed, Muhammad Maaz, Sahal Shaji, Abdelrahman Shaker, Salman Khan, Hisham Cholakkal, Rao M Anwer, Eric Xing, Ming-Hsuan Yang, and Fahad S Khan. Glamm: Pixel grounding large multimodal model. In *Proceedings of the IEEE/CVF Conference on Computer Vision and Pattern Recognition*, pages 13009–13018, 2024. 2, 6, 7
- [29] Nikhila Ravi, Valentin Gabeur, Yuan-Ting Hu, Ronghang Hu, Chaitanya Ryali, Tengyu Ma, Haitham Khedr, Roman Rädle, Chloe Rolland, Laura Gustafson, et al. Sam 2: Segment anything in images and videos. *arXiv preprint arXiv:2408.00714*, 2024. 4, 6
- [30] Zhongwei Ren, Zhicheng Huang, Yunchao Wei, Yao Zhao, Dongmei Fu, Jiashi Feng, and Xiaojie Jin. Pixellm: Pixel reasoning with large multimodal model. In *Proceedings of the IEEE/CVF Conference on Computer Vision and Pattern Recognition*, pages 26374–26383, 2024. 2, 6, 7
- [31] John Schulman, Filip Wolski, Prafulla Dhariwal, Alec Radford, and Oleg Klimov. Proximal policy optimization algorithms. *arXiv preprint arXiv:1707.06347*, 2017. 3
- [32] Zhihong Shao, Peiyi Wang, Qihao Zhu, Runxin Xu, Junxiao Song, Xiao Bi, Haowei Zhang, Mingchuan Zhang, YK Li, Yang Wu, et al. Deepseekmath: Pushing the limits of mathematical reasoning in open language models. *arXiv preprint arXiv:2402.03300*, 2024. 1, 4
- [33] Haozhan Shen, Peng Liu, Jingcheng Li, Chunxin Fang, Yibo Ma, Jiajia Liao, Qiaoli Shen, Zilun Zhang, Kangjia Zhao, Qianqian Zhang, et al. Vlm-r1: A stable and generalizable r1-style large vision-language model. *arXiv preprint arXiv:2504.07615*, 2025. 1, 2
- [34] Guangming Sheng, Chi Zhang, Zilingfeng Ye, Xibin Wu, Wang Zhang, Ru Zhang, Yanghua Peng, Haibin Lin, and Chuan Wu. Hybridflow: A flexible and efficient rlhf framework. *arXiv preprint arXiv: 2409.19256*, 2024. 6, 1
- [35] Peng Wang, Shuai Bai, Sinan Tan, Shijie Wang, Zhihao Fan, Jinze Bai, Keqin Chen, Xuejing Liu, Jialin Wang, Wenbin Ge, et al. Qwen2-vl: Enhancing vision-language model’s perception of the world at any resolution. *arXiv preprint arXiv:2409.12191*, 2024. 6, 7, 2, 4
- [36] Song Wang, Gongfan Fang, Lingdong Kong, Xiangtai Li, Jianyun Xu, Sheng Yang, Qiang Li, Jianke Zhu, and Xinchao Wang. Pixelthink: Towards efficient chain-of-pixel reasoning. *arXiv preprint arXiv:2505.23727*, 2025. 2, 3, 6, 7
- [37] Shenzhi Wang, Le Yu, Chang Gao, Chujie Zheng, Shixuan Liu, Rui Lu, Kai Dang, Xionghui Chen, Jianxin Yang, Zhenru Zhang, et al. Beyond the 80/20 rule: High-entropy minority tokens drive effective reinforcement learning for llm reasoning. *arXiv preprint arXiv:2506.01939*, 2025. 2, 3
- [38] Zhiqiang Wang, Pengbin Feng, Yanbin Lin, Shuzhang Cai, Zongao Bian, Jinghua Yan, and Xingquan Zhu. Crowdvlm-r1: Expanding r1 ability to vision language model for crowd counting using fuzzy group relative policy reward. *arXiv preprint arXiv:2504.03724*, 2025. 2
- [39] Fang Wu, Weihao Xuan, Ximing Lu, Zaid Harchaoui, and Yejin Choi. The invisible leash: Why rlvr may not escape its origin. *arXiv preprint arXiv:2507.14843*, 2025. 2
- [40] Zhuofan Xia, Dongchen Han, Yizeng Han, Xuran Pan, Shiji Song, and Gao Huang. Gsva: Generalized segmentation via multimodal large language models. In *Proceedings of the IEEE/CVF Conference on Computer Vision and Pattern Recognition*, pages 3858–3869, 2024. 2, 6, 7
- [41] Senqiao Yang, Tianyuan Qu, Xin Lai, Zhuotao Tian, Bohao Peng, Shu Liu, and Jiaya Jia. Lisa++: An improved baseline for reasoning segmentation with large language model. *arXiv preprint arXiv:2312.17240*, 2023. 6, 2
- [42] Shuo Yang, Yuwei Niu, Yuyang Liu, Yang Ye, Bin Lin, and Li Yuan. Look-back: Implicit visual re-focusing in mllm reasoning. *arXiv preprint arXiv:2507.03019*, 2025. 5
- [43] Zhao Yang, Jiaqi Wang, Yansong Tang, Kai Chen, Hengshuang Zhao, and Philip HS Torr. Lavt: Language-aware vision transformer for referring image segmentation. In *Proceedings of the IEEE/CVF conference on computer vision and pattern recognition*, pages 18155–18165, 2022. 1, 6, 7
- [44] En Yu, Kangheng Lin, Liang Zhao, Jisheng Yin, Yana Wei, Yang Peng, Haoran Wei, Jianjian Sun, Chunrui Han, Zheng Ge, et al. Perception-r1: Pioneering perception policy with reinforcement learning. *arXiv preprint arXiv:2504.07954*, 2025. 2
- [45] Licheng Yu, Patrick Poirson, Shan Yang, Alexander C Berg, and Tamara L Berg. Modeling context in referring expressions. In *European conference on computer vision*, pages 69–85. Springer, 2016. 6, 2
- [46] Haotian Zhang, Haoxuan You, Philipp Dufter, Bowen Zhang, Chen Chen, Hong-You Chen, Tsu-Jui Fu, William Yang Wang, Shih-Fu Chang, Zhe Gan, et al. Ferret-v2: An improved baseline for referring and grounding with large language models. *arXiv preprint arXiv:2404.07973*, 2024. 4
- [47] Shilong Zhang, Peize Sun, Shoufa Chen, Min Xiao, Wenqi Shao, Wenwei Zhang, Yu Liu, Kai Chen, and Ping Luo. Gpt4roi: Instruction tuning large language model on region-of-interest. In *European conference on computer vision*, pages 52–70. Springer, 2024. 1
- [48] Tao Zhang, Xiangtai Li, Hao Fei, Haobo Yuan, Shengqiong Wu, Shunping Ji, Chen Change Loy, and Shuicheng Yan. Omg-llava: Bridging image-level, object-level, pixel-level reasoning and understanding. *Advances in neural information processing systems*, 37:71737–71767, 2024. 1, 2, 6, 7

- [49] Zheng Zhang, Yeyao Ma, Enming Zhang, and Xiang Bai. Psalm: Pixelwise segmentation with large multi-modal model. In *European Conference on Computer Vision*, pages 74–91. Springer, 2024. 1
- [50] Yaowei Zheng, Junting Lu, Shenzhi Wang, Zhangchi Feng, Dongdong Kuang, and Yuwen Xiong. Easyrl: An efficient, scalable, multi-modality rl training framework. <https://github.com/hiyouga/EasyRl>, 2025. 1

Dr. Seg: Revisiting GRPO Training for Visual Large Language Models through Perception-Oriented Design

Supplementary Material

We provide supplementary material related to the main paper, arranged as follows:

1. More Experiment Details and Ablations (Section A)
2. Qualitative Results (Section B)
3. Additional Results on REC (Section C)
4. Dataset Details (Section D)

A. More Experiment Details and Ablations

Details of Dr. Seg. Our project is built on SAM [15], VERL [34], EasyR1 [50], and VisionReasoner [25]. The global batch size is 16, with the micro batch size per device for updates and the micro batch size per device for experience collection both set to 2. The rollout number per sample is 8, and the KL-loss coefficient is 1×10^{-2} . We use the AdamW optimizer with a learning rate of 1×10^{-6} and a weight decay of 1×10^{-2} .

Details of VisionReasoner with Raw Reward. In Sec. 3.3, we replace the binary rewards in VisionReasoner with unnormalized continuous rewards. Concretely, for the box IoU reward, we directly use the continuous IoU value without applying any threshold. For the box L1 reward and point L1 reward, we adopt the same linear scaling function in Eq.15. All other settings are kept the same as in the original VisionReasoner configuration.

COCO Precision/Recall Metrics. Following VisionReasoner [25], we compute mAP by assigning each predicted box a proxy score defined as the ratio of the predicted box area to the image area. We also evaluate Precision/Recall/F1 to avoid such approximation.

Method	AP@0.5	P@0.5	R@0.5	F1
Qwen2-VL	43.5	72.1	41.3	52.5
Qwen2.5-VL	47.6	72.4	46.6	56.7
VisionReasoner	57.3	62.6	63.9	63.3
Dr. Seg	59.0	69.6	64.3	66.8

Table 7. More detection metrics on COCO.

Ablation on Response Length. To isolate whether the gains come from simply generating longer responses, we compare several test-time prompting variants that increase the average response length while keeping the underlying model unchanged. As shown in Tab. 8, merely elongating the output does not improve performance: both a generic Chain-of-Thought prompt and a Look-to-Confirm style prompt substantially increase the response length but degrade gIoU (e.g., $65.5 \rightarrow 63.1$ and 59.6). In contrast,

Dr. Seg achieves the best gIoU (67.8) with a similar length range, indicating that the improvement cannot be attributed to longer responses. Length denotes the word count, measured on the ReasonSeg val set.

Method	Length	gIoU
Baseline	77.8	65.5
+ Chain-of-Thought prompt	117.0	63.1
+ Look-to-Confirm prompt	137.3	59.6
Dr. Seg	148.3	67.8

Table 8. Ablation on response length using test-time prompts.

Ablation on Format Reward. To further verify whether the gain could come from a particular output structure (e.g., the $\langle \text{look} \rangle$ tag) or learned semantic guidance, We conduct a controlled ablation that matches structure by retraining with the same format reward R_{format} , while changing the keyword inside the tag (e.g., $\langle \text{look} \rangle$, $\langle \text{wait} \rangle$) or using unrelated keywords. As shown in Tab. 9, adding R_{format} with random/wait keywords yields only marginal changes (64.9–65.6 gIoU), suggesting that format constraints alone are insufficient. Moreover, removing R_{format} (Look*) fails to stably generate the tag and degenerates toward the baseline, indicating R_{format} is necessary for stable structured behavior.

Keyword	R_{format}	Length	gIoU
Random	✓	89.6	64.9
Wait	✓	95.3	65.6
Look*		73.6	65.8
Look	✓	148.3	67.8

Table 9. Ablation on response structure by retraining with/without the format reward R_{format} and varying the tag keyword. Look*: without R_{format} , the model fails to stably generate $\langle \text{look} \rangle$ and degrades toward the baseline.

Ablation on Accuracy Reward Components. To clarify the contribution of each accuracy component, we ablate the reward composition used in R_{accuracy} by progressively adding x_1 (IoU), x_2 (count), and x_3 (point) in Tab. 10.

B. Qualitative Results

We provide a qualitative example in Fig. 8 and more visualizations in Fig. 12. As illustrated in Fig. 8, prior methods [25] struggle in complex multi-object segmentation scenarios, often miscounting target instances due to over- or

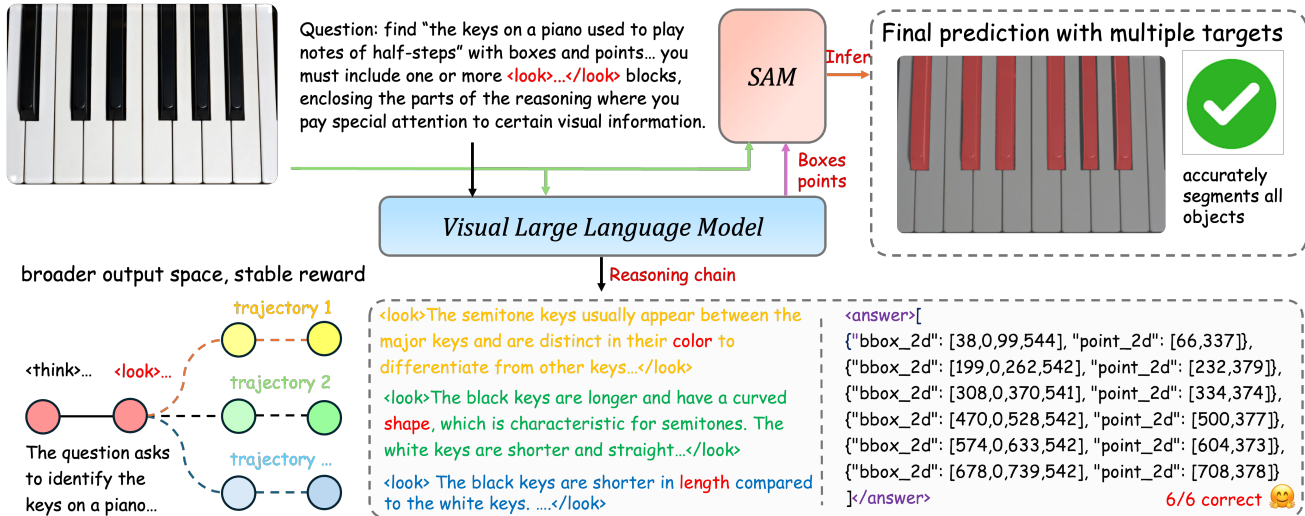


Figure 8. Supplementary illustration of the Dr. Seg architecture. The model first performs a Look-to-Confirm exploration, generating multiple reasoning trajectories that describe diverse visual cues. During inference, these trajectories are used to prompt SAM to produce mask proposals. The example shown here demonstrates successful segmentation of all six semitone keys (6/6 correct).

Setting	RefCOCO testA	ReasonSeg val
w	35.6	24.1
$w x_1$	72.9	57.8
$w x_1, x_2$	79.8	58.3
$w x_1, x_2, x_3$	80.2	67.8

Table 10. Ablation on R_{accuracy} .

under-segmentation. For example, in the piano half-step case, the baseline model correctly identifies only 4 out of 6 candidate keys. We argue that these errors stem from two coupled factors: (1) binary rewards fail to reflect fine-grained performance differences, providing only coarse supervision; and (2) the restricted output space limits the model’s ability to explore diverse reasoning trajectories, causing incorrect object enumeration. Our method alleviates these issues: the proposed Look-to-Confirm mechanism expands the model’s output space by encouraging exploration of alternative visual cues, while the Distribution-Ranked Reward delivers stable fine-grained feedback independent of metric scales. Together, these components yield substantially more accurate object counts. We provide more visualizations in Fig. 12, highlighting the effectiveness of our method in challenging multi-object settings.

C. Additional Results on REC

We also evaluate our models’ performance on the referring expression comprehension (REC) task, with results reported in Tab. 12. Our model also achieves superior performance compared with previous methods [25] and base models [1, 35]. Specifically, it outperforms the baseline Vi-

sionReasoner on all three REC datasets, with an average improvement of 0.7 absolute points.

D. Dataset Details

Training Dataset Statistics. We use the *VisionReasoner_multi_object_7k.840* dataset [25], which was constructed by the authors of VisionReasoner from four sources: LVIS [13], RefCOCOg [45], gRefCOCO [19], and LISA++ [41]. It is formed by sampling roughly 1,800 examples from the training split of each dataset, without any special data partitioning criteria, resulting in a balanced mixture across the four sources.

Evaluation Dataset Statistics. Table 11 summarizes the statistics of all evaluation datasets used in this study. For a fair comparison, we follow prior work [24, 25] and adopt the same data splits as in their experiments; we report the number of evaluation samples. The benchmark suite covers (i) referring expression segmentation (RefCOCO, RefCOCO+, RefCOCOg [45]); (ii) reasoning-oriented segmentation (ReasonSeg [16]); (iii) our self-constructed multi-object split (COCONut; details in the next paragraph); (iv) object detection (MS COCO [18]); (v) object counting (Pixmo-Count [8], CountBench [26]) and (vi) referring expression comprehension (RefCOCO, RefCOCO+, RefCOCOg).

Evaluation Metrics. For object detection on COCO, we adopt the standard AP metric computed using the COCO API. For referring expression comprehension on RefCOCO series, we use bbox AP, which measures detection accuracy at an IoU threshold of 0.5. For object segmentation on Re-

fCOCO series and ReasonSeg, we use gIoU, computed as the mean IoU across all segmentation masks. For counting tasks, we use count accuracy as the evaluation metric.

Table 11. Statistics of evaluation benchmarks. Numbers combine validation and test splits where applicable. DET, REC, SEG, and CNT denote Detection, Referring Expression Comprehension, Referring Expression Segmentation, and Counting, respectively.

Dataset	Split	# of samples
DET	COCO	36,781
REC	RefCOCO	5,786
	RefCOCO+	5,060
	RefCOCOg	7,596
SEG	RefCOCO	1,975
	RefCOCO+	1,975
	RefCOCOg	5,023
	ReasonSeg	979
	COCONut	665
CNT	Pixmo-Count	1,064
	CountBench	504
SUM		67,408

Details of COCONut Benchmark. Since publicly avail-

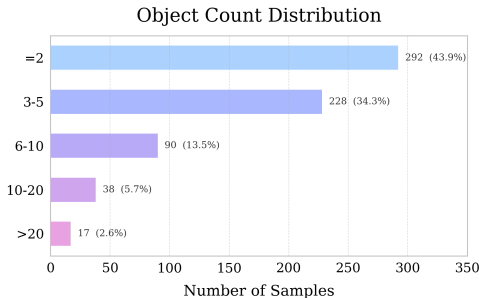


Figure 9. Object count distribution of the COCONut multi-object split.

able datasets for complex, multi-object segmentation remain scarce, we additionally construct a benchmark from COCONut val split [10], a dataset that couples panoptic segmentation with grounded captions.

Sampling Protocol. We sample 1,000 images from the official validation split and, after filtering, retain 665 images. The procedure is as follows:

1. **Candidate filtering:** We discard images without annotations. For each remaining image, we count per-class instance frequencies and keep only those images in which at least one class appears at least twice. For each retained



Figure 10. Categories included in our COCONut dataset, all of which are subclasses of the original COCO label set.

image, we collect the set of classes that satisfy this criterion and randomly choose one target class from this set.

2. **Union-mask construction:** For the chosen class, we build a binary mask for every instance of that class and take the pixel-wise OR over all such masks to obtain the class-level union mask across the full image.
3. **Text prompt:** For each sample, we form the instruction All <category>, indicating “segment all instances of the specified class.”
4. **Quality Control:** Finally, we perform a light manual pass to remove low-quality cases (e.g., extremely small targets or ambiguous class references). The remainder constitutes our dataset.

Goal and Characteristics. This benchmark evaluates class-level multi-instance union reasoning: given a natural image and a concise class prompt, the model must output the combined region covering all instances of that class. Unlike typical single-instance prompts, this setting stresses coverage completeness over multiple same-class objects, which better reflects crowded or overlapping real-world scenes. We also provide summary statistics and qualitative examples in Fig. 9 and Fig. 11.

Table 12. Performance on the referring expression comprehension task.

Method	Referring Expression Comprehension						avg
	RefCOCO		RefCOCO+		RefCOCog		
	val	testA	val	testA	val	test	
Task-specific Models							
DQ-DETR [22]	88.6	91.0	81.7	86.2	82.8	83.4	85.6
Grounding-DINO-T(ft) [23]	89.2	91.9	81.1	87.4	84.2	84.9	86.5
Grounding-DINO-L(ft) [23]	90.6	93.2	82.8	89.0	86.1	87.0	88.1
7B Visual Large Language Models							
Qwen2-VL [35]	80.8	83.9	72.5	76.5	77.3	78.2	78.2
Qwen2.5-VL [1]	88.8	91.7	82.3	88.2	84.7	85.7	86.9
Shikra [2]	87.0	90.6	81.6	87.4	82.3	82.2	85.2
Ferret-v2 [46]	87.5	91.3	80.8	87.4	83.9	84.8	86.0
InternVL2-8B [4]	87.1	91.1	79.8	87.9	82.7	82.7	85.2
VisionReasoner [25]	88.6	90.6	83.6	87.9	86.1	87.5	87.4
Dr. Seg (Ours)	89.4	91.5	83.6	88.0	88.1	88.0	88.1

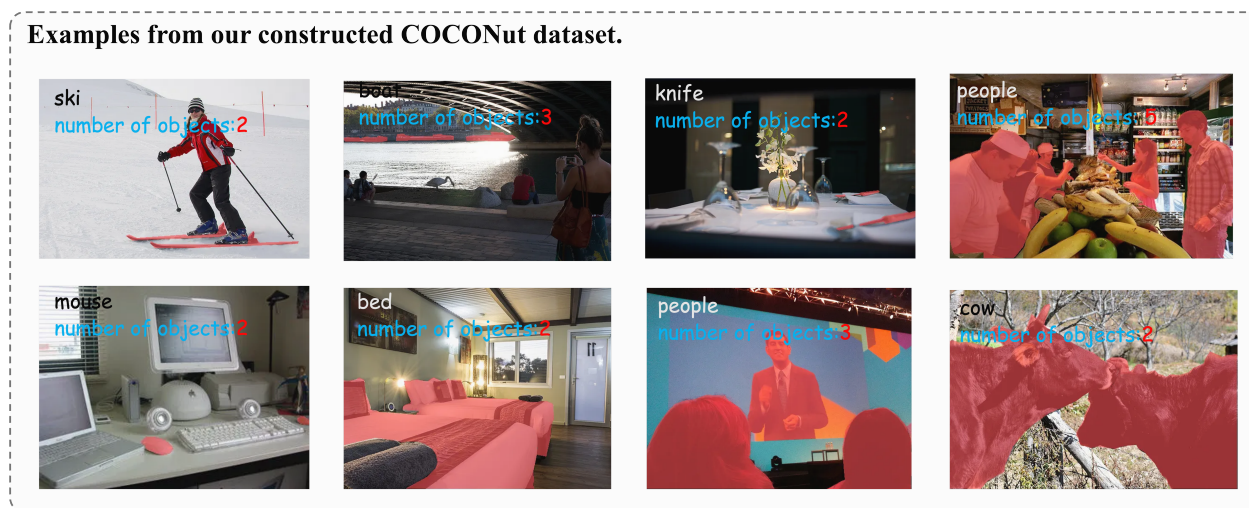


Figure 11. Visualization of our COCONut dataset, illustrating diverse object categories and a wide range of object counts per image.

Examples of our method compared with previous.



VisionReasoner: <think> The person in the image is the one with bare arms, which is the biker riding the bike in the foreground. The other biker riding the purple bike is wearing a t-shirt and jeans, which might not necessarily be bare arms, but still, they also could be a close match. The two people visible are the two bikers.</think><answer>[{"bbox_2d": [262,83,385,300], "point_2d": [283,179]}, {"bbox_2d": [363,135,553,528], "point_2d": [417,289]}]</answer>



Dr. Seg (Ours): <think> [The person with bare arms is the one riding the motorcycle in the foreground. They are wearing a sleeveless shirt, which suggests they have bare arms. The other person is wearing a helmet and appears to be moving away from the camera, wearing a full jacket, which might cover their arms partially.] <look> [The person in the foreground is clearly not wearing a shirt, showing their bare arms, which aligns with the description of having bare arms. The other person is distanced and dressed differently, with a helmet, which makes it less likely for them to have bare arms.] </look> There might be another potential match for someone with bare arms in the background, but observing their attire and distance from the camera, they do not seem to fit the description as well.</think><answer>[{"bbox_2d": [263,84,385,301], "point_2d": [289,183]}]</answer>



Figure 12. A representative failure case of prior methods. The model initially attends to the correct person but drifts away as the chain-of-thought unfolds, leading to over or under counting the target instances. We attribute this behavior to excessive noise in the reward design: collapsing raw rewards into binary signals discards information and introduces noise. This noise is then further amplified when heterogeneous metric scales are summed together.

Examples of our method compared with previous.

Origin image

Visionreasoner

Dr. Seg (ours)

Question: " the person with the highest status"



<think> [The person with the highest status in a Tibetan Buddhist context, typically a monk, is often dressed in yellow robes, which can be seen in the image. However, it's important to consider the context and the surrounding statues, as the individual seated prominently might also have a significant position within the community. The statue behind the group, though, appears to be a Buddha statue, which could imply that the individual is not a monk but a religious leader or a respected figure in the Buddhist community.] <look> [The yellow-robed figure is positioned behind the group, suggesting a higher status within the context of Tibetan Buddhism, which may not match the individual identified as having the highest status within the image.] </look> Therefore, the person wearing the yellow robe might be the one with the highest status.] </think><answer>[{"bbox_2d": [318,159,481,472], "point_2d": [410,304]}]</answer>

Question: " What object in the picture can be used to display the names and prices?"



<think> [The image shows a bunch of fish with yellow labels on them, which contain prices. These labels are the most relevant objects for displaying names and prices of different fish. They are typically used in fish markets to provide information to potential buyers. The rest of the fish and the table they are placed on are not directly used to display the information.] <look> [The labels are rectangular yellow tags with black text that contain numerical values presumably representing prices, and they are directly visible on the fish, which are the primary elements being sold. The labels are designed to quickly convey important information to the audience in the context of a fish market.] </look> The labels can be used to display the names and prices of different fish in a fish market setting.] </think><answer>[{"bbox_2d": [2,139,107,265], "point_2d": [49,207]}, {"bbox_2d": [101,190,222,363], "point_2d": [167,288]}, {"bbox_2d": [210,147,327,258], "point_2d": [270,209]}, {"bbox_2d": [335,172,474,290], "point_2d": [404,235]}, {"bbox_2d": [499,147,616,289], "point_2d": [582,234]}, {"bbox_2d": [662,165,783,233], "point_2d": [730,200]}, {"bbox_2d": [809,137,839,137], "point_2d": [399,95]}, {"bbox_2d": [309,367,466,590], "point_2d": [392,485]}, {"bbox_2d": [629,375,740,518], "point_2d": [698,450]}, {"bbox_2d": [180,456,315,688], "point_2d": [248,569]}]</answer>

Figure 13. Visualization of the proposed Dr. Seg compared with VisionReasoner.

Examples of our method compared with previous.

Origin image

Visionreasoner

Dr. Seg (ours)

Question: " Some people enjoy having a view of the outside world while still being comfortable inside their homes. What part of the house in the picture can provide such an experience?"



<think> [The part of the house with a bay window allows people to enjoy a view of the outside world while being comfortable inside. The bay window design in the image suggests that it is a larger window that protrudes from the wall, providing ample natural light and an expansive view of the surroundings. The presence of ivy and the curved design of the window emphasize the aesthetic appeal of this feature, making it a pleasant and functional space for homeowners.] <look> [The window and the view outside would be the prominent objects for someone to enjoy the outside while remaining inside. The bay window, with its curved elements, can provide a unique and interesting view for the inhabitants, while the greenery outside suggests a pleasant environment to view.] </look> The most closely matched object in the image is the window.</think><answer>[{"bbox_2d": [362,164,505,569], "point_2d": [434,357]}, {"bbox_2d": [528,180,649,576], "point_2d": [596,396]}, {"bbox_2d": [209,171,334,571], "point_2d": [275,340]}]</answer>

Question: " someone who is most likely to be the player"



<think> [The person wearing a black shirt, white pants, and a helmet is likely the player because they are dressed appropriately for a baseball player and are positioned on the field where players typically are. The other individuals, while also present in the scene, do not have the typical attire or position of a baseball player, indicating that the one with the helmet is the most likely player.] <look> [The visual focus is on the person with the helmet, who is wearing a baseball outfit and is positioned as a potential player, which suggests they are the one most likely to be the player in the game. The other individuals either do not have the necessary attire or are not in the correct position on the field to be considered players at this moment.] </look> The person with the helmet and baseball outfit is most likely the player.</think><answer>[{"bbox_2d": [422,42,631,763], "point_2d": [573,275]}]</answer>

Figure 14. More visualization of the proposed Dr. Seg compared with VisionReasoner.